Mon. Not. R. Astron. Soc. **334,** 673–683 (2002)

The 2dF Galaxy Redshift Survey: the environmental dependence of galaxy star formation rates near clusters

Ian Lewis,[1,2] Michael Balogh,[3⋆] Roberto De Propris,[4] Warrick Couch,[4] Richard Bower,[3] Alison Offer,[2] Joss Bland-Hawthorn,[2] Ivan K. Baldry,[5] Carlton Baugh,[3] Terry Bridges,[2] Russell Cannon,[2] Shaun Cole,[3] Matthew Colless,[6] Chris Collins,[7] Nicholas Cross,[6,8] Gavin Dalton,[1] Simon P. Driver,[6,8] George Efstathiou,[9] Richard S. Ellis,[10] Carlos S. Frenk,[3] Karl Glazebrook,[2] Edward Hawkins,[11] Carole Jackson,[6] Ofer Lahav,[9] Stuart Lumsden,[12] Steve Maddox,[11] Darren Madgwick,[9] Peder Norberg,[3] John A. Peacock,[13] Will Percival,[13] Bruce A. Peterson,[6] Will Sutherland[13] and Keith Taylor[10]

[1]*Astrophysics, Nuclear and Astrophysics Laboratory, Keble Road, Oxford OX1 3RH*
[2]*Anglo-Australian Observatory, PO Box 296, Epping, NSW 1710, Australia*
[3]*Department of Physics, University of Durham, South Road, Durham DH1 3LE*
[4]*School of Physics, University of New South Wales, Sydney 2052, Australia*
[5]*Department of Physics and Astronomy, Johns Hopkins University, 3400 North Charles Street, Baltimore, MD 21218-2686, USA*
[6]*Research School of Astronomy & Astrophysics, The Australian National University, Weston Creek, ACT 2611, Australia*
[7]*Astrophysics Research Institute, Liverpool John Moores University, Twelve Quays House, Egerton Wharf, Birkenhead, L14 1LD*
[8]*School of Physics and Astronomy, University of St. Andrews, North Haugh, St. Andrews, Fife KY16 9SS*
[9]*Institute of Astronomy, University of Cambridge, Madingley Road, Cambridge*
[10]*California Institute of Technology, Pasadena, CA 91125-2400, USA*
[11]*School of Physics and Astronomy, University of Nottingham, University Park, Nottingham, NG7 2RD*
[12]*Department of Physics & Astronomy, E C Stoner Building, Leeds LS2 9JT*
[13]*Institute for Astronomy, University of Edinburgh, Royal Observatory, Edinburgh EH9 3HJ*

Accepted 2002 March 28. Received 2002 March 28; in original form 2002 February 7

ABSTRACT

We have measured the equivalent width of the Hα emission line for 11 006 galaxies brighter than $M_b = -19$ ($\Omega_\Lambda = 0.7$, $\Omega_m = 0.3$, $H_0 = 70$ km s^{-1} Mpc^{-1}) at $0.05 < z < 0.1$ in the 2dF Galaxy Redshift Survey (2dFGRS), in the fields of 17 known galaxy clusters. The limited redshift range ensures that our results are insensitive to aperture bias, and to residuals from night sky emission lines. We use these measurements to trace μ^*, the star formation rate normalized to L^*, as a function of distance from the cluster centre, and local projected galaxy density. We find that the distribution of μ^* steadily skews toward larger values with increasing distance from the cluster centre, converging to the field distribution at distances greater than $\sim$3 times the virial radius. A correlation between star formation rate and local projected density is also found, which is independent of cluster velocity dispersion and disappears at projected densities below $\sim$1 galaxy Mpc^{-2} (brighter than $M_b = -19$). This characteristic scale corresponds approximately to the mean density at the cluster virial radius. The same correlation holds for galaxies more than two virial radii from the cluster centre. We conclude that environmental influences on galaxy properties are not restricted to cluster cores, but are effective in all groups where the density exceeds this critical value. The present-day abundance of such systems, and the strong evolution of this abundance, makes it likely that hierarchical growth of structure plays a significant role in decreasing the global average star formation rate. Finally, the low star formation rates well beyond the virialized cluster rule out severe physical processes, such as ram pressure stripping of disc gas, as being completely responsible for the variations in galaxy properties with environment.

Key words: galaxies: clusters: general.

⋆E-mail: m.l.balogh@durham.ac.uk

1 INTRODUCTION

The effect of local environment on galaxy evolution in general is not well understood. Studies of environmental effects in the past have been largely devoted to the study of galaxies in the cores of rich clusters, which differ so dramatically from more common galaxies (e.g. Dressler 1980; Dressler, Thompson & Shectman 1985; Couch & Sharples 1987; Balogh et al. 1997, 1999; Poggianti et al. 1999; Moss & Whittle 2000; Couch et al. 2001; Solanes et al. 2001). However, galaxies in cluster cores comprise only a small fraction of the stellar content within the Universe, and thus it is not obvious that the processes which effect these galaxies are important for galaxy evolution in general.

More recently, however, work has begun to show that star formation is suppressed in cluster galaxies far from the core. From the CNOC1 cluster sample, Balogh et al. (1997, 1998) found that the mean cluster galaxy star formation rate may be suppressed as far as twice the virial radius (R_v) from the cluster centre, relative to a field sample selected in the foreground and background of the clusters. However, the data at large radii were sparse, and being derived from only a few clusters were sensitive to the effects of substructure and non-sphericity. Thus it is not possible to draw strong conclusions about the relative cluster galaxy star formation rate beyond the R_v from these data. Wide field photometric analysis of clusters using Subaru has recently suggested that the tight red sequence of early-type galaxies first presents itself in small groups of galaxies within the infall region of the massive cluster Cl0939 + 47 at $z = 0.39$ (Kodama et al. 2001). This is the first work to suggest that a 'critical' environment for galaxy evolution exists. A larger survey, designed specifically to study the outer regions of clusters, is the Las Campanas/Anglo-Australian Observatory Rich Cluster Survey (LARCS), a sample of 17 rich, X-ray bright clusters, with photometry and spectroscopy extending out to very large radii (∼6 Mpc). Early results confirm the radial gradient in photometric and spectroscopic properties out to the virial radius and, perhaps, beyond (O'Hely 2000; Pimbblet et al. 2001a,b).

It therefore seems likely that galaxy star formation rates are reduced before they are accreted by a cluster, for example in smaller groups. If this is the case, the implications could be profound, as most galaxies at the present day are in groups (Turner & Gott 1976; Geller & Huchra 1983; Tully 1987; Carlberg et al. 2001); if environmental processes are important in these regions, they will clearly be reflected in the evolution of the universe as a whole. As structure builds up in the Universe, more and more galaxies can be found in groups and, if these environments serve to terminate star formation, the mean star formation rate of the Universe will decline. This might explain at least part of the observed decline in global star formation with cosmic time (Lilly et al. 1996; Madau et al. 1996; Cowie, Songaila & Barger 1999).

The 2dF Galaxy Redshift Survey (2dFGRS) allows the unprecedented opportunity to study the spectroscopic properties of galaxies at an arbitrarily large distance from any given cluster. The details of the survey strategy are given elsewhere (Colless et al. 2001), but summarized briefly in Section 2.1. Analysis of the whole sample will allow a definitive study of any correlation between spectral properties (i.e. emission line strength) as a function of a continuous variable like local density. For this preliminary study, we are specifically interested in establishing precisely where galaxies in the vicinity of known clusters begin to exhibit properties which differ from those of the average galaxy. We base this on a sample of 17 known rich clusters within the 2dFGRS, from the catalogue of De Propris et al. (2002).

Our cluster selection, galaxy sample and star formation rate measurements are described in Section 2. In Section 3 we show the trend of increasing star formation activity with both increasing clustercentric distance, and decreasing local projected density. This is compared with numerical models in Section 4. We summarize our findings in Section 5. Throughout this paper, we use a cosmology with $\Omega_\Lambda = 0.7$, $\Omega_m = 0.3$ and $H_0 = 70$ km s^{-1} Mpc^{-1}. We use the symbol M_b to denote absolute magnitudes measured in the 2dFGRS photographic blue system.

2 DATA ANALYSIS

2.1 Spectroscopic data

The 2dF Galaxy Redshift Survey has obtained over 220 000 spectra of galaxies located in two contiguous declination strips, plus 99 randomly located fields. One strip is in the southern Galactic hemisphere and covers approximately $80^\circ \times 15^\circ$ centred close to the Super Galactic Plane (SGP). The other strip is in the northern Galactic hemisphere and covers $75^\circ \times 10^\circ$. The 99 random fields are located over the entire region of the Automated Plate Measuring Facility (APM) galaxy catalogue in the southern Galactic hemisphere outside of the main survey strip. Full details of the survey strategy are given in Colless et al. (2001).

The survey spectra cover the wavelength range 3600–8000 Å at 9-Å resolution. Only the wavelength range of 3600–7700 Å is used during the line fitting procedure, owing to the poor signal to noise ratio and strong sky emission in the red part of the spectrum. The wide wavelength range is made possible by the use of an atmospheric dispersion compensator (ADC) within the 2dF instrument (Lewis et al. 2002).

2.2 Cluster selection

We select 17 clusters from the catalogue of De Propris et al. (2002), in which clusters from the Abell catalogues (Abell 1958; Abell, Corwin & Olowin 1989), the APM (Dalton et al. 1997) and the EDCC (Lumsden et al. 1992) were cross-referenced with the 2dFGRS. This catalogue is still partially incomplete, but the completeness is generally better than 75 per cent within ∼5 Mpc of the cluster centres. The mean redshift and velocity dispersions of the clusters in this catalogue have been recomputed from the 2dFGRS spectra, and the cluster centroid is taken to be the brightest cluster galaxy with early-type morphology, identified from Palomar Observatory Sky Survey (POSS) plates.

For this analysis, we extract from the 2dFGRS all galaxies within ∼20 Mpc of the centre of 17 clusters, selected to lie at $18\,000 < cz < 29\,000$ km s^{-1}. The lower velocity bound is chosen to limit the angular size to a reasonably small, manageable value; the upper limit is defined as the velocity at which Hα is redshifted into the first set of strong night-sky OH emission lines. 10 clusters were selected to have velocity dispersions $\sigma > 800$ km s^{-1}, while the remaining seven are systems with $400 < \sigma < 800$ km s^{-1}. The redshift histograms for the 17 clusters, including all galaxies brighter than $M_b = -19$ within 5 Mpc (projected) of the centre, are shown in Fig. 1. Details of the clusters, including their redshifts (cz), velocity dispersions (σ), number of cluster members brighter than $M_b = -19$, and completeness (within 5 Mpc), are summarized in Table 1. De Propris et al. (2002) resolved Abell 1238 into two clusters aligned along the line of sight; we here consider the lower redshift cluster, designated Abell 1238L. The cluster centres and velocity dispersions are generally better determined than they appear

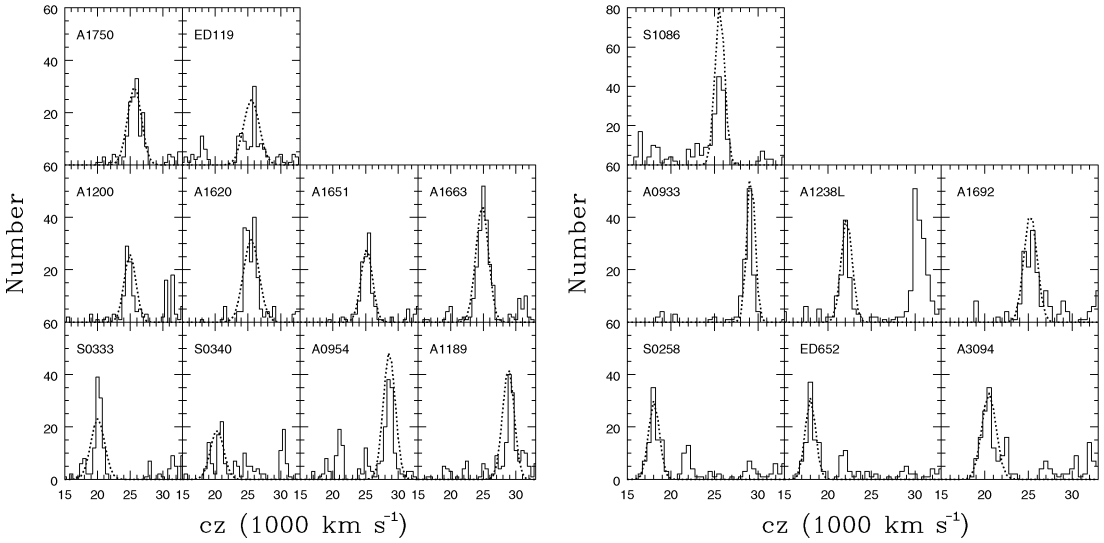

Figure 1. Redshift histograms for the seventeen clusters used in this study. Only galaxies brighter than $M_b = -19$ and within 5 Mpc of the cluster centre are included. The dotted line overlayed on each histogram represents a Gaussian with a central redshift (cz) and velocity dispersion as tabulated in Table 1. Left: the 10 clusters with velocity dispersion $\sigma > 800$ km s^{-1}. Right: the remaining seven clusters with $\sigma < 800$ km s^{-1}.

Table 1. The 17 clusters used in this study.

Name	(B1950)		cz	$N_{\rm mem}$	σ	Completeness	$R_{\rm v}$	$R_{\rm v}$ (alt.)
	R.A. ($^{\rm h}$ $^{\rm m}$ $^{\rm s}$)	Dec. ($^\circ$ $'$ $''$)	(km s^{-1})		(km s^{-1})	(within 5 Mpc)	(Mpc)	(Mpc)
S0258	02:23:33.21	−29:50:26.9	18060	31	583	0.72	1.6	1.9
ED652	02:25:11.88	−29:51:00.7	18001	21	564	0.75	1.4	1.8
A3094	03:09:16.42	−27:07:08.4	20475	63	774	0.84	2.0	2.4
S0333	03:13:04.34	−29:25:41.3	20042	40	998	0.90	1.6	3.2
S0340	03:17:55.68	−27:11:45.6	20281	18	939	0.87	1.2	3.0
A0933	10:05:14.50	+00:45:25.7	29180	72	420	0.54	2.4	1.3
A0954	10:11:11.10	+00:07:40.2	28622	74	832	0.77	2.2	2.5
A1189	11:08:30.14	+01:21:42.6	28824	51	814	0.77	1.9	2.5
A1200	11:10:03.25	−02:56:27.6	24970	38	825	0.83	1.7	2.6
A1238L	11:20:20.36	+01:23:19.4	22160	53	586	0.82	1.9	1.8
A1620	12:47:29.78	−01:16:07.1	25513	51	1095	0.89	1.8	3.4
A1651	12:56:47.48	−03:55:36.9	25152	46	817	0.47	2.1	2.5
A1663	13:00:18.05	−02:14:57.7	24827	75	884	0.80	2.1	2.7
A1692	13:09:41.25	−00:39:59.7	25235	49	686	0.80	1.8	2.1
A1750	13:28:36.52	−01:28:15.9	25647	83	981	0.62	2.4	3.0
ED119	22:13:32.57	−25:55:10.7	25546	38	1112	0.84	1.7	3.4
S1086	23:02:06.51	−32:49:14.8	25605	74	502	0.53	2.4	1.5

in Fig. 1, as they are computed including fainter galaxies over a smaller projected area (where the contrast with the field is greater).

2.3 Hα measurements

All of the measurements of equivalent width have been performed using a completely automatic procedure. For each spectrum we remove the continuum by subtracting the median over a 133-Å (31-pixel) wide window after first excluding known absorption and emission line regions by making use of the known galaxy redshift. Bad pixels and sky line residuals and the atmospheric and fibre absorption bands are also excluded from the continuum fitting.

Both emission and absorption lines are fitted with Gaussian profiles which are adequate for most of the emission lines and cores of the absorption lines. Up to 20 individual absorption and emission lines are fitted simultaneously using a modified Levenberg–Marquardt algorithm. The width and height of each line are fitted together with a small perturbation of the observed redshift. Some lines were constrained to be emission or absorption. Others were allowed to be either. Note that the relative wavelength spacing of all lines remains fixed, but the fitted redshift is allowed to vary slightly (typically $\Delta z \sim 0.00025$, and always $\Delta z < 0.005$). By fitting many lines simultaneously we avoid individual line fits shifting to the nearest available peak or dip in the spectrum. By fitting both absorption and emission lines we ensure that the method is robust to the redshift solution, whatever type of spectrum is being fitted.

With this technique of simultaneous line fitting it is possible to allow for line blends by simply requesting two or more lines to be fitted to the blend. For example Hβ is best fitted by a combination of a narrow emission and a broad absorption line, and the Hα emission line can be accurately deblended from the adjacent [N II]λ6548 Å and [N II]λ6583 Å lines, despite the 9-Å resolution of the spectra. The [N II] lines are constrained to be in emission while the Hα line may be either emission or absorption. To fit the Gaussian profile

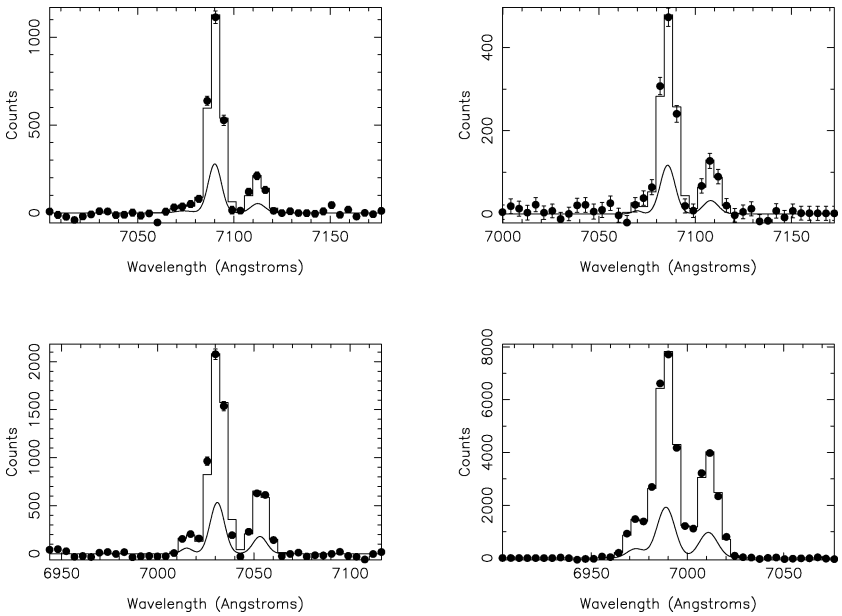

Figure 2. Four examples of the Gaussian line-fits to the spectra, for varying strengths of [N II] and signal-to-noise ratio. Each plot shows the observed low resolution data as a series of filled circles with rms error bars. The modelled Gaussian fit is shown as a smooth curve and the modelled Gaussian sampled at the same resolution as the observed data is shown as a histogram.

to the data points, a consideration has to be made for the effect of the undersampling of the data. The solution is to model a Gaussian profile which, when undersampled, fits the observed data closely. Fig. 2 shows the resulting fit for four spectra with varying [N II]/Hα ratios, and demonstrates the effect of the undersampling.

After line fitting, the parameters of the fit (amplitude, σ and area) and the rms residuals are used to classify the quality of the line fit. Usual reasons for rejecting a fit are if the line is too narrow (e.g. a noise spike or residual cosmic ray hit), or too broad (for a forbidden line). Some combinations of lines are also rejected, for example Hα absorption combined with [N II] emission. Lines which are too weak for a good fit are also flagged; however they are not rejected from the analysis, so that we retain a dispersion in the flux which reflects the measurement uncertainties. Partial failures are flagged often as a result of large rms residuals to the fit (broad non-thermal emission lines are poorly fitted by Gaussian profiles) or a poor wavelength calibration at the blue end of the spectrum, which can lead to a poor line profile for [O II]. The latter is usually the case when the observed spectrum was close to the edge of the CCD. Care is also taken when a bad pixel has been masked out from the spectrum within 2σ of the line centroid.

Equivalent widths (EWs) are then simply calculated using the continuum fit and the measured line flux. A small number of spectra are degraded by poor sky subtraction at the data reduction stage, which can result in a negative continuum, making the EW meaningless. These cases can be easily removed from subsequent analysis.

2.4 Sample selection and star formation rates

2dFGRS spectra within 20 Mpc of each cluster centre were extracted from the data base. The extreme ends of spectra taken earlier than 1999 August are severely affected by problems with the ADC (Lewis et al. 2002); hence we restrict our analysis to data taken after this date. This leaves us with 53 018 galaxies, but to limit the effect of aperture bias and sky-subtraction residuals, we restrict the sample to those galaxies which lie within $0.05 < z < 0.1$. Within this redshift range, the galaxy sample is complete to $M_b = -19$, and we adopt this as our luminosity limit. This leaves us with 12 020 galaxies. For computations of star formation rates, we exclude galaxies in which the continuum was negative, or a Gaussian was a poor fit to the line (see Section 2.3). This removes an additional 734 galaxies from the sample ($\sim$6 per cent). Finally, for galaxies with a significant Hα equivalent width ($W_{\rm H\alpha} > 10$ Å), we exclude galaxies in which the equivalent width of the adjacent [N II]λ6583 line is greater than $0.55W_{\rm H\alpha}$. These 280 galaxies (2.3 per cent of the sample) are likely to have a significant non-thermal component (Veilleux & Osterbrock 1987). This leaves us with a final sample of 11 006 galaxies. We take cluster members to be those within 3σ, where σ is the cluster velocity dispersion determined by De Propris et al. (2002), shown in Table 1. The number of such members within the virial radius (see below) is denoted $N_{\rm mem}$ in the table. Note that for the three highest redshift clusters A0933, A0954 and A1189, the highest velocity members are not included as a result of our overall redshift cut ($0.05 < z < 0.1$); however, all galaxies within 2σ are still available. 5829 galaxies in our final sample are thus defined as cluster members.

Kennicutt (1983, 1992) derived a conversion from Hα luminosity to star formation rate, under the assumptions of Case B recombination, no escape of Lyman α photons, and a Salpeter-like initial mass function. This may underestimate the current star formation rate by a small factor, due to extinction in the line-emitting regions (Charlot & Longhetti 2001). Also, if the nature of star formation is burst-like, the instantaneous star formation rate may not be representative of the average over even short ($\sim$100 Myr) time-scales (Sullivan et al. 2001). However, neither of these effects are likely to affect a comparison of galaxy populations with similar luminosity functions, as is the case in the present work.

As the 2dFGRS spectra are not flux-calibrated, we cannot derive Hα luminosities, or star formation rates. However, after making a small (2 Å) correction for the underlying stellar absorption, we can use the EWs to calculate the star formation rate normalized to a fiducial luminosity (essentially a star formation rate per unit

normalized luminosity). If μ is the star formation rate in units of $M_\odot$ yr^{-1} and $L_{H\alpha}$ is the total luminosity of the Hα emission line in erg s^{-1}, we can define

$$\eta = \mu / L_{H\alpha}. \quad (1)$$

We will use the 'average' conversion factor of $\eta = 7.9 \times 10^{-42}$ $M_\odot$ s yr^{-1} erg^{-1}(Kennicutt 1992). The equivalent width of Hα, corrected for stellar absorption, is given by

$$W_{H\alpha} \approx L_{H\alpha} / L_c, \quad (2)$$

where L_c is the continuum luminosity in units of erg s^{-1} Å^{-1}. We can then calculate μ^* as

$$\mu^* = \frac{\mu}{L_c / L^*} = \eta W_{H\alpha} L^*, \quad (3)$$

where L^* is a characteristic luminosity, for normalization, in units of erg s^{-1} Å^{-1}. We take L^* to correspond to the knee in the luminosity function in the r' band (near rest-frame Hα), as determined by Blanton et al. (2001), $M_R = -21.8$ ($\Omega_\Lambda = 0.7$, $\Omega_m = 0.3$, $h = 0.7$), or $L^* = 1.1 \times 10^{40}$ erg s^{-1} Å^{-1}. Therefore, we have

$$\mu^* = 0.087 W_{H\alpha}, \quad (4)$$

which gives the star formation rate, in units of $M_\odot$ yr^{-1}, normalized to L^*.

We measure the projected distance of each galaxy from the cluster, as defined by the brightest central galaxy. In some cases the cluster membership of a galaxy is ambiguous, because it lies within 20 Mpc and the 3σ redshift limits of more than one cluster (e.g. clusters S0258 and ED652). In this case, the galaxy is assumed to belong to the cluster which is nearest in projected distance.

In order to put all the clusters (which span more than a factor of 2 in velocity dispersion) on a common scale, and to facilitate comparison with theory, we need to relate projected distances to the virial radius, R_v, of the cluster. We show the spatial distribution of the cluster members within 1° of the centre for each cluster in Fig. 3. From this figure it is evident that many of our clusters are not spherically symmetric. Thus we must be cautious in our interpretation of R_v as a physically meaningful scale, particularly when considering individual clusters.

The definition of R_v is

$$\bar{\rho}(<R_v) = \Delta_c(z)\rho_c(z) = \Delta_c(z)\rho_b(z)/\Omega_m(z), \quad (5)$$

where $\bar{\rho}(<R_v)$ is the mean cluster mass density within R_v, ρ_c and ρ_b are the critical density and mean background mass density, respectively, and Δ_c is the redshift-dependent contrast parameter, determined from spherical collapse theory. For a flat $\Omega_m = 1$ universe, $\Delta_c = 178$; for our adopted cosmology at $z = 0.07$, $\Delta_c \approx 107$ (Eke, Cole & Frenk 1996), and $\Omega_m(z) = 0.343$, so $\Delta_c(z)/\Omega_m(z) = 312$. We will assume that the number density of galaxies is directly proportional to the dark matter density, independent of scale or galaxy luminosity. In this case, we can take the mean background density ρ_b from the luminosity function. Integrating the best-fitting Schechter function from Cross et al. (2001), we find that the number density of galaxies brighter than $M_b = -19$ is $\rho_b = 0.0076$ Mpc^{-3} ($h = 0.7$). We determine $\bar{\rho}(<R_v)$ by counting the number of cluster members N within R_v (weighting by the completeness given in Table 1) and assuming a spherical cluster geometry, so $\bar{\rho}(<R_v) = 3N/(4\pi R_v^3)$. Substituting this into equation (5), we need to solve $R_v = 0.465 N^{1/3}$. This is done iteratively, by first estimating R_v, counting the number of members N within R_v, and then

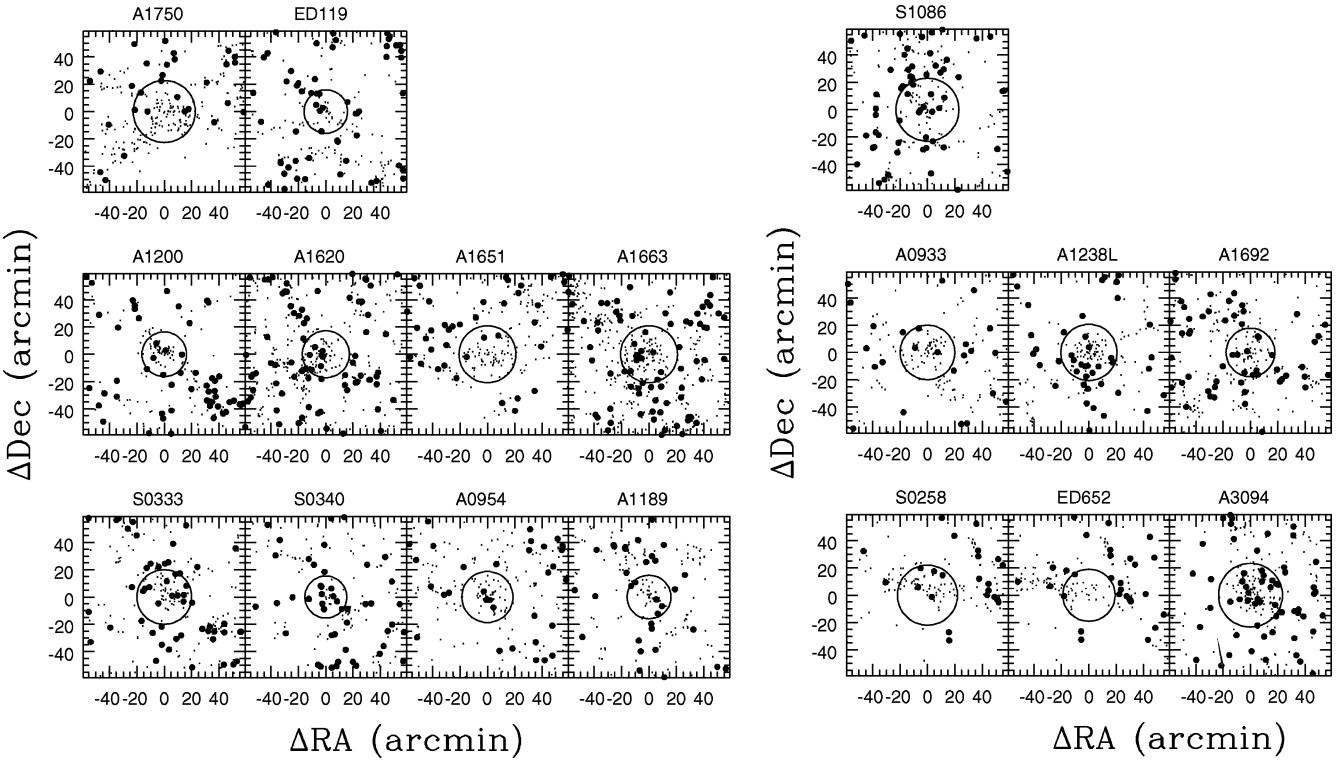

Figure 3. Spatial distributions for cluster members within 1° of the cluster centre. The filled circles are galaxies with $W_{H\alpha} > 20$ Å. The large circle in each panel traces the estimated virial radius for the cluster. Left: the 10 clusters with velocity dispersion $\sigma > 800$ km s^{-1}. Right: the remaining seven clusters with $\sigma < 800$ km s^{-1}.

recomputing R_v. This is repeated until the solution converges, usually within ∼3 iterations. These measurements of R_v are given in column 7 of Table 1.

Alternatively, the virial radius can be determined directly from the velocity dispersion, under various assumptions, as outlined in Girardi et al. (1998). If M_v is the virialized mass, and R_v is the cluster virial radius, we have

$$\Delta_c = \frac{3M_v}{4\pi\rho_c R_v^3}. \quad (6)$$

The virial mass can be related to the velocity dispersion σ and R_v under the assumption of spherical symmetry, through

$$M_v = 3G^{-1}\sigma^2 R_v, \quad (7)$$

so we have

$$R_v = \frac{3\sigma}{\sqrt{4\pi G\rho_c\Delta_c}} = \sqrt{\frac{6}{\Delta_c}}\sigma/H_0. \quad (8)$$

For either a flat, $\Omega_m = 1$ cosmology (with $h = 0.5$) or the Ω_Λ-dominated cosmology we have adopted ($h = 0.7$), the virial radius in Mpc is $R_v \approx 3.5\sigma(1+z)^{-1.5}$, for σ in units of 1000 km s^{-1}.

For nine of the 17 clusters, this calculation [listed as 'R_v (alt.)' in Table 1] agrees with the previous one to within ∼20 per cent. For most of the remaining cases, where there is a large discrepancy between the two measurements of R_v, the velocity histograms are significantly non-Gaussian, and thus the velocity dispersion is likely to be a poor tracer of the mass. For this reason, we will always adopt the first calculation of R_v as the most likely to be correct. Moreover, this occasional discrepancy, and the non-Gaussianity of the corresponding velocity histograms, likely implies that the computed velocity dispersions are not always simply related to the virialized mass. For example, some clusters (ED119, S0333, S0340) may have velocity dispersions which are artificially inflated by the presence of foreground and background structures. Thus, our division of the sample into two based on velocity dispersion may not reflect a perfect division into low- and high-mass clusters.

We will draw the reference field population from the 2400 galaxies more than 6σ from the cluster redshift, i.e. in the foreground and background of the clusters. As a result of the small redshift range considered, $0.05 < z < 0.1$, and the use of an absolute luminosity limit, the field sample is also volume limited. The luminosity function of the field sample is comparable to that of the cluster sample, as shown in Fig. 4 (see also De Propris et al. 2002).

3 RESULTS

3.1 General cluster properties

In Fig. 5 we show the distribution of normalized star formation rate, μ^*, in the cluster and field samples, excluding galaxies with relatively strong [N II]λ6583 emission (see Section 2.4). The cluster sample is limited to the 440 members within R_v, while the field sample is drawn from the 2400 galaxies beyond 6σ in velocity. The difference between the distributions is highly significant,[1] with the field galaxy population weighted toward galaxies with stronger star formation.

[1] The probability that the two distributions are not drawn from the same population is >99.999 per cent as determined by a Kolmogorov–Smirnov test.

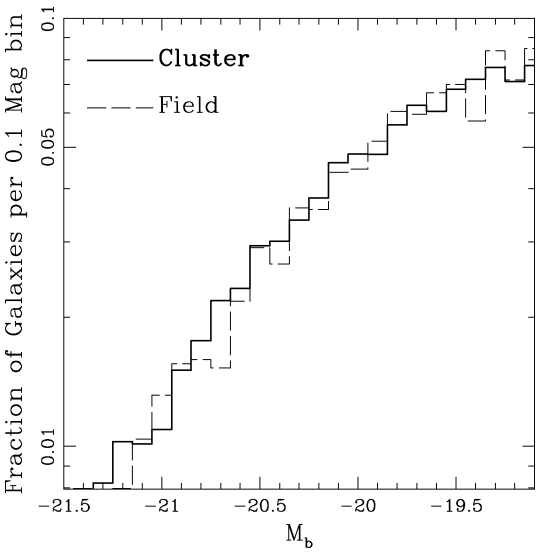

Figure 4. Luminosity functions of the cluster sample (solid histogram) and the field sample (dashed histogram).

3.2 Radial dependences

It is well known that star formation activity in clusters increases with distance from the centre (Balogh et al. 1997, 1998, 1999). In Fig. 6 we show how the mean and median value of μ^* depend on radius in our cluster sample, and compare that with the field value. We also show, in the third panel, the fraction of galaxies with $\mu^* > 1$, which represent the tail of the distribution, comprised of galaxies that are currently forming stars at a high rate relative to their luminosity. The sample is also broken up into clusters with high ($\sigma > 800$ km s^{-1}, triangles) and low ($\sigma < 800$ km s^{-1}, crosses) velocity dispersions. The properties of the field sample are shown by the horizontal, solid line. The dashed lines bracketing the field line represent the 1σ standard deviation from field to field, computed by ordering the field galaxies in right ascension and treating every 200 galaxies as an individual sample. This gives some estimate of the expected cosmological variance in the field value.

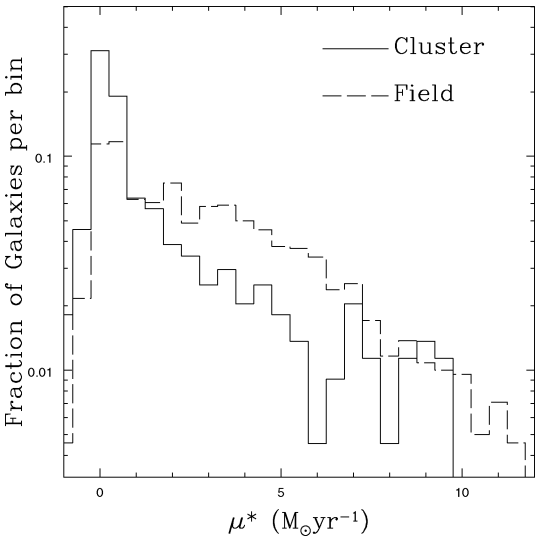

Figure 5. The distribution of star formation rate per unit luminosity, in the cluster and field samples. The cluster sample is limited to galaxies within the virial radius.

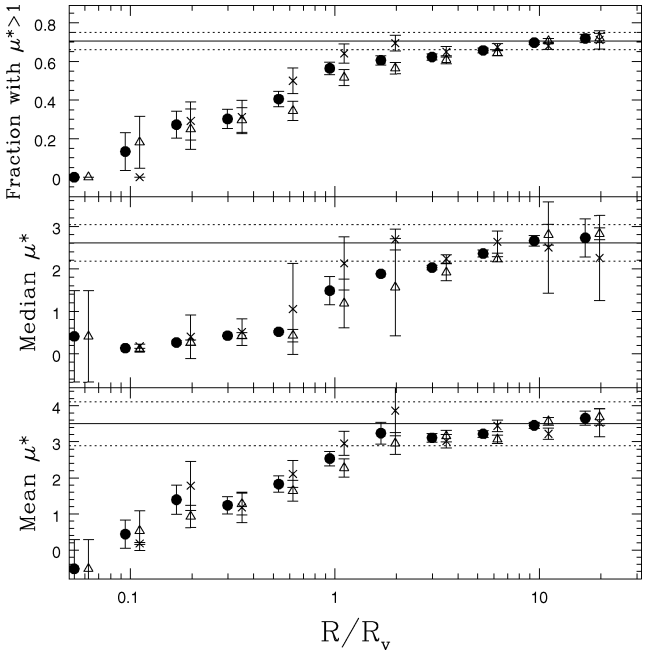

Figure 6. The mean (bottom panel) and median (middle panel) value of μ^* in the cluster sample, as a function of radius. In the top panel we show the fraction of galaxies with $\mu^* > 1$ $M_\odot$ yr^{-1}. Error bars are a jackknife resampling estimate. Solid points represent the full galaxy sample, while the triangles and crosses represent only the clusters with σ greater than or less than 800 km s^{-1}, respectively (offset for clarity). Only points in which the radial bin contains at least three galaxies are shown. The horizontal, solid line represents the value of each statistic in the field sample. The dotted lines which bracket the line are an estimate of the 1σ field-to-field standard deviation, for independent samples of 200 galaxies.

All three statistics demonstrate that the cluster distribution of μ^* becomes equivalent to the field value only well outside the virial radius, at $R \gtrsim 3R_v$, in excellent agreement with preliminary results from the Sloan Digital Sky Survey (Gomez et al. 2002). The implications of this are that a representative sample of field galaxies cannot be obtained within $\lesssim$6 Mpc of the cluster core. Thus, photometric studies of clusters which attempt a statistical background subtraction by taking the field from the cluster outskirts (e.g. Kodama & Bower 2001; Pimbblet et al. 2001b) are not subtracting enough star-forming galaxies, and artificially inflating the number of blue galaxies within the cluster.

Because many of the clusters are not spherically symmetric, the interpretation of radial gradients, and the physical meaning of R_v, is not straightforward. From Fig. 3 it is clear that there is often considerable structure, both within and without the virial radius. Furthermore, the galaxies with strongest Hα emission (solid points in Fig. 3) appear to be spread evenly throughout the field, avoiding the densest regions, regardless of cluster-centric distance. Thus, in the following section we consider the correlation between star formation rate and local density.

3.3 Density dependences

There has been controversy over whether or not galaxy populations correlate most closely with cluster-centric radius (Whitmore, Gilmore & Jones 1993) or local density (Dressler 1980; Postman & Geller 1984). If radius is the primary determinant anywhere, it is most likely only within the very central regions of the cluster (Domínguez, Muriel & Lambas 2001). Studies which stack many clusters to approximate a spherically symmetric supercluster circumvent this difficulty, as average density becomes a monotonic function of radius within R_v (e.g. Balogh et al. 1997, 1998). In our case, the outer regions of the clusters often contain several large groups or other clusters of galaxies (see Fig. 3). Thus, it is probably more appropriate to consider the local density of the galaxies as the most physically interesting variable.

To compute the local density of cluster members, we consider all galaxies in the spectroscopic catalogue (including those with bad ADC or Hα measurements) brighter than $M_b = -19$, and within 3σ of the cluster redshift. We then take the distance to the tenth-nearest galaxy, in projected radius, as r_{10}; the local projected density is then $\Sigma = 10/\pi r_{10}^2$. For galaxies near the boundary of a cluster catalogue, this will underestimate the true density. To partially account for this, we only consider galaxies within 18 Mpc of the cluster centre, so they are at least 2 Mpc from the edge of the catalogue. In some cases, however, the current 2dFGRS data base is incomplete within the 20 Mpc extracted area, and the densities of galaxies near these incomplete regions will still be underestimated.

In Fig. 7 we show the distribution of density, for galaxies in three radial bins. In the cluster centre, almost all galaxies are in regions of very high local density. However, at large radii galaxies can be found in a wide range of environments; in particular it is not uncommon to find galaxies at $R > 3R_v$ with local densities as large as those within the virialized region. Within the virial radius, the distribution of Σ is similar for both high and low velocity dispersion clusters; the means are the same within ∼5 per cent, and the probability that both distributions are drawn from the same population is 0.12 as determined by a Kolmogorov–Smirnov test. Between $1 < R_v < 5$, however, there is a significant (>99.999 per cent) difference, and the mean local density of the clusters with $\sigma > 800$ km s^{-1} is more than twice as large as that of the lower velocity dispersion clusters.

In Fig. 8, we show the properties of the cluster μ^* distribution, as in Fig. 6, but plotted against Σ. The vertical line shows the mean projected density of galaxies within the virial radius, $N(<R_v)/\pi R_v^2$ (note that this is not the same as the average of the Σ values calculated for each galaxy). As in Fig. 6, the horizontal lines show

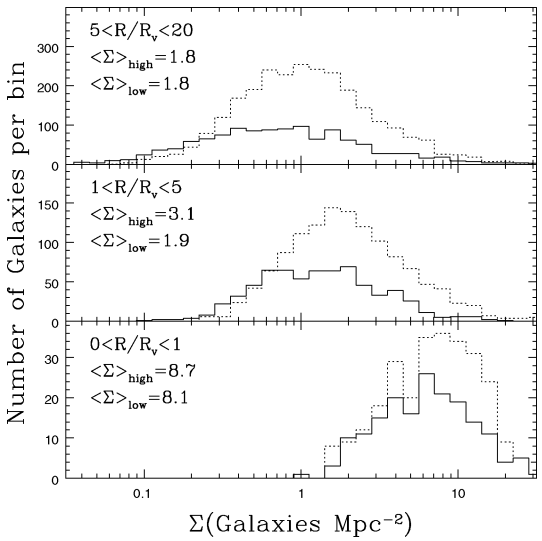

Figure 7. The local, projected density distribution of galaxies in different radial bins as labelled. Clusters with $\sigma > 800$ km s^{-1} are shown as the dotted line, and the mean value is shown in the top left corner as Σ_{high}. The solid line represents clusters with $\sigma < 800$ km s^{-1}; their mean value is Σ_{low}.

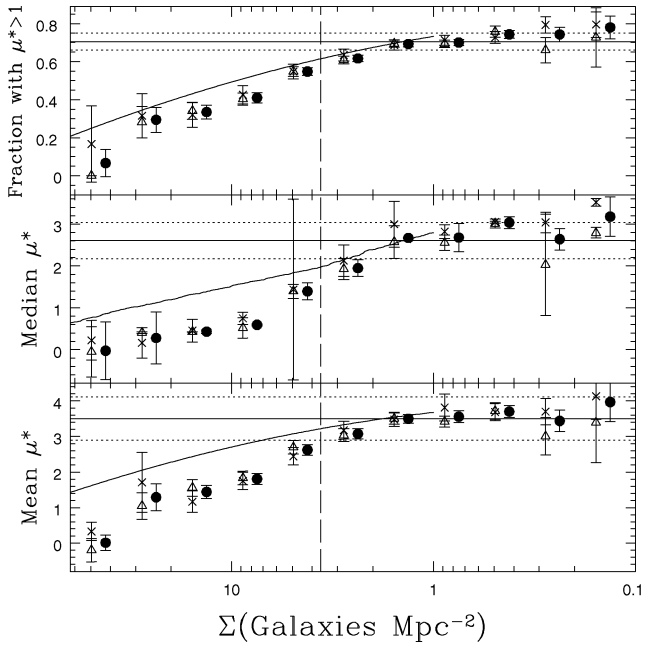

Figure 8. As Fig. 6, but as a function of local projected density. The vertical, dashed line represents the mean projected density of galaxies within the virial radius of the cluster. The solid curves (discussed in Section 4.1) are the expected trends due to the morphology–density relation of Dressler (1980), assuming the field population is composed of 18 per cent E, 23 per cent S0 and 59 per cent spiral galaxies (Whitmore et al. 1993).

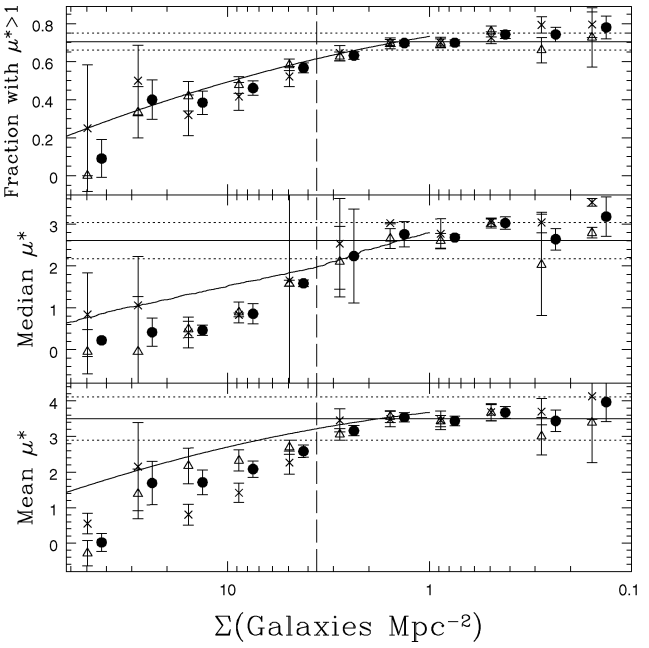

Figure 9. As Fig. 8, but restricted to galaxies beyond $2R_v$.

the values of each statistic in the field. The field actually spans a range of densities, probably similar to that seen far ($>5R_v$) from the cluster centre (see Fig. 7); however, our density estimate in clusters is a measure of the galaxy density projected along a line-of-sight column of unknown length, and thus cannot be directly applied to field galaxies to obtain a comparable measurement of local density. Thus, it is evident that star formation is suppressed at densities of $\Sigma \sim 1.5$ galaxies Mpc^{-2}, approximately 2.5 times lower than the mean projected density of the cluster virialized region.

As in Fig. 6, the star formation rate distribution at a given density is similar in both high- and low-velocity dispersion clusters. This suggests that galaxy star formation rates depend only on the local density, regardless of the larger-scale structure in which they are embedded, although we repeat our caution that the velocity dispersions may not be directly related to the cluster mass in all cases. Furthermore, as we show in Fig. 9, the correlation of star formation rate with density holds at $r > 2R_v$, well outside the virialized cluster region. This demonstrates that star formation is low relative to the global average in *any* region exceeding the critical density of 1 galaxy Mpc^{-2} (brighter than $M_b = -19$), regardless of its proximity to a rich cluster (see also Postman & Geller 1984).

4 DISCUSSION

4.1 Comparison with the morphology–density relation

We have shown that the dependence of star formation rate on local galaxy density is independent of cluster velocity dispersion and thus, presumably, mass (see Section 3.3). In a recent photometric study based on *Hubble Space Telescope* imaging of 17 clusters, Balogh et al. (2002) found some evidence that the morphology–density relation *does* depend on cluster X-ray luminosity, which is likely to be a better tracer of mass than velocity dispersion; at a given local density, low-mass clusters have more disc-dominated galaxies than high-mass clusters. Furthermore, they showed that this is most probably due to a difference in the population of galaxy bulges; the disc luminosity function at a fixed local density does not depend on cluster mass. Since star formation is generally limited to the galaxy disc, our results are consistent with this picture. The luminosity of a disc, and its star-forming activity, depend only on galaxy density, while the luminosity of the bulge component has an additional, small dependence on the mass of the embedding structure.

It would be of great interest to compare the dependence of μ^* on density with the similar density-dependence of morphology, to determine the degree to which the two correlations are independent. In particular, any difference between the two shows that cluster galaxies differ from their morphological counterparts in the field, which supports the hypothesis that they have undergone a physical transformation (Balogh et al. 1998). However, we note that this test is not conclusive; if the star formation rate of a spiral galaxy is reduced gradually, on time-scales similar to that for morphological change, the correlation between morphology and star formation rate may be retained, despite the transformation.

Unfortunately, morphological classifications are not yet available for our sample. However, we can use the local morphology–density relation computed by Dressler (1980), assuming that it is universal. The luminosity limit of our sample ($M_b = -19$) is similar to that of Dressler, $M_b \approx -19.2$, after accounting for the difference in cosmology and making the transformation $M_b = M_V + 0.72(B-V)$, assuming an average galaxy colour $B-V = 0.8$ (Fukugita, Shimasaku & Ichikawa 1995). Thus, our density measurements should be comparable. We will assume that the field galaxy sample is composed of 18 per cent E, 23 per cent S0 and 59 per cent spiral and irregular galaxies (Whitmore et al. 1993; Dressler et al. 1997). We therefore divide the field galaxy μ^* distribution (Fig. 5) into three populations, identifying the lowest 18 per cent of μ^* values with the E population, the next 23 per cent with the S0s, and the remainder with spirals. It is then straightforward to recompute the

statistics shown in Fig. 8 for any morphological mix. We show the expected μ^*–density relation computed in this way, assuming Dressler's morphology–density relation, as the solid curves in Fig. 8. Two things are immediately clear. First, at $\Sigma = 1$ Mpc^{-2}, the lowest density point in Dressler's study, the cluster morphological mix is close to that adopted for the field, so the predicted curve is in good agreement with our measurements. Note that this is dependent on an accurate determination of the early-type fraction in the field, estimates of which have increased from the 20 per cent adopted by Dressler (1980), to 30 per cent (Sandage & Tammann 1981) adopted by Postman & Geller (1984), and finally to the 41 per cent used here and elsewhere (Whitmore et al. 1993; Dressler et al. 1997). This high value for the early-type fraction is a consequence of the bright luminosity limit, and is consistent with that derived from type-dependent luminosity functions of Marzke et al. (1994, 40 per cent at M^*). The second point is that the predicted μ^*–density correlation appears to be shallower than the observed relation. This suggests that the morphology–density relation may be distinct from the star formation–density relation. In making this comparison we have made the extreme assumption that the lowest values of μ^* are associated with elliptical galaxies, and the highest values with spiral galaxies. Any dispersion in the natural morphology–μ^* relation will serve to further flatten the predicted μ^*–density relation and increase the discrepancy with the data. On the other hand, there is an important caveat, as Dressler (1980) did not subdivide the late-type morphology class, and Sa galaxies are known to have much less current star formation than irregular galaxies (Kennicutt 1992; Jansen et al. 2000). If the fraction of Sa galaxies relative to later types increases with density, this will steepen the curves in Fig. 8.

4.2 Possible mechanisms: comparison with theoretical models

These results show conclusively that suppressed star formation is not limited to the cores of rich clusters, but is found in any environment in which the local projected galaxy density exceeds one galaxy brighter than $M_b = -19$ per Mpc^2. This is in approximate agreement with the results of Kodama et al. (2001), though a direct comparison is not possible because that survey probes much deeper down the luminosity function, so the local projected galaxy densities are higher in the same environments. Whatever mechanism is responsible for terminating star formation in galaxies, then, is not particular to the cores of rich clusters, but is associated with dense groups in the cluster infall regions as well. This means that ram pressure stripping of galaxy discs cannot be completely responsible for the correlation of star formation with local density, as this is only expected to take place in the cores of rich clusters (Gunn & Gott 1972; Fujita 2001; Quilis, Moore & Bower 2000).

Most hierarchical models of galaxy formation do not include a calculation of ram-pressure stripping of the cold, disc gas, nor of other physical processes like galaxy harassment (Moore et al. 1999) which might play a role in dense environments. The only environmental effect on star formation rate in these models – apart from a possible difference in merging history – is related to the hot, halo gas hypothesized to surround every isolated galaxy. It is assumed that galaxies maintain the supply of cold gas – fuel for star formation – via continuous cooling from a hot, diffuse gas halo associated with the dark matter potential (Somerville & Primack 1999; Kauffmann et al. 1999; Cole et al. 2000). In haloes with more than one galaxy, this hot gas is only associated with the central galaxy; satellite galaxies are assumed to lose their supply of fresh fuel through ram pressure stripping and tidal effects (though these are not directly modelled). In these models, therefore, star formation rates begin to decline for any satellite galaxy, whether in a poor group or a rich cluster.

These models are able to reproduce radial gradients in star formation within the virial radius of clusters to a remarkably high degree of accuracy (Diaferio et al. 2001; Okamoto & Nagashima 2001). In particular, Diaferio et al. (2001) predict that the mean star formation rate should be equivalent to the field value beyond $\sim 2R_v$, in physical (i.e. not projected) space. The model of Balogh, Navarro & Morris (2000) is a greatly simplified version of this more complete model, as the properties of the field galaxy population are not modelled directly, but are taken empirically from observations of the $z \sim 0.3$ field. The advantage is that the effects of the halo-stripping can be seen directly, as that is the only physical process (apart from gravity) which is accounted for. In Fig. 10, we show the predictions of this model, for the mean star formation rate relative to the field, as a function of local projected density. The simulations on which the model is based were kindly provided by Julio Navarro. Here, local density is defined as the projected surface mass density, computed by finding the radius encompassing the 10 nearest (in projection) particles in the simulations. The model is the 'group' model in fig. 1 of Balogh et al. (2000); galaxies are assumed to lose their reservoir of hot gas when they are associated with a group with circular velocity $V_c > 600$ km s^{-1}. While a direct comparison with the data is not possible, since these simulations only provide the dark matter density, a comparison relative to the mean surface density within R_v should be fair if mass traces light. First we note that the approximately power-law dependence on local projected density has a similar slope in the data and the model; the mean star formation rate decreases by a factor of ~ 3 for every factor of 10 increase in surface density. Secondly, in the model the correlation flattens out at surface densities $\sim 1/7$ times that of the mean projected density within R_v. Although this threshold is a factor of ~ 2 lower than seen in the data, given the crudity of the model, we consider the agreement

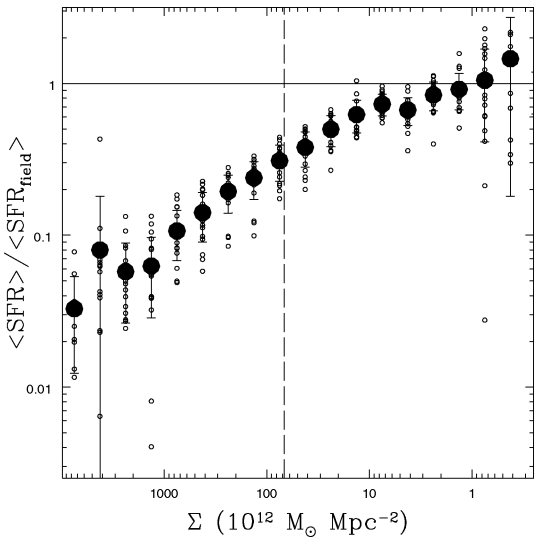

Figure 10. The 'group' model of Balogh et al. (2000), in which galaxies in groups with circular velocity $V_c > 600$ km s^{-1} have their hot gas haloes stripped, so no further cooling is permitted. The density is the local projected mass density, computed from the area enclosing the nearest ten particles in projection. Small, open points are results from a single projection of each of six model clusters; the large solid point is the mean, and the error bar is the standard deviation of the 18 realizations of the model. The dashed line shows the mean density of particles within the virial radius.

reassuring. Unfortunately, the simulations used in this model did not include a large enough volume to probe beyond a few R_v. Thus, the low density regions in the simulations are not drawn from the same regions in space as the low density regions in the observations, most of which are found well beyond $2R_v$.

Thus, models in which halo-stripping is the only direct environmental-influence on the galaxy star formation rate provide a reasonably good match to the data. This is especially remarkable given that the stripping is not even directly modelled; it is simply assumed that every satellite galaxy has *no* reservoir of hot gas, immediately after it merges with a larger halo. Improvement in this respect alone may well improve the models' success in the lower density regions, far from the cluster core.

4.3 Consequences on the evolution of the global star formation rate

What mechanisms are responsible for driving the strong observed evolution of the global star formation rate (e.g. Lilly et al. 1996)? One possibility is that the decline in star formation activity is related to physics internal to individual galaxies – for example, consumption of a limited gas supply, or a time-dependent cooling rate – regardless of their environment. On the other hand, some of the decline is likely to be tied to the hierarchical growth of structure; as time progresses, more and more galaxies are locked up in clusters where, perhaps, star formation is directly inhibited.

According to extended Press–Schechter theory (Bower 1991; Bond et al. 1991) the fraction of mass in haloes greater than 10^{14} $M_\odot$, approximately the limit of our cluster sample, is only 11 per cent at the present day, and negligible by $z = 1$. Thus it is not immediately obvious that the lower star formation rates in these systems can have any effect on the global average. However, we have shown that lower star formation rates are seen in environments with densities $\sim$0.3 times lower than the mean cluster density, regardless of their proximity to the cluster. This density corresponds approximately to the density *at* the virial radius; by definition, if mass traces light then any virialized structure will have a mean density which exceeds this threshold. Because our density estimate is based on the tenth-nearest galaxy brighter than $M_b = -19$, we cannot be sure how our results apply to systems with fewer than 10 such galaxies. A virialized system with more than 10 galaxies brighter than this limit is expected to have a total gravitational mass $M \gtrsim 10^{13}$ $M_\odot$, assuming a total mass-to-light ratio of 100 (e.g. Girardi et al. 2002). In contrast with the more massive clusters, these haloes account for $\sim$35 per cent of the mass in the present day Universe, and contribute significantly to the global average star formation rate. Furthermore, at $z = 1$ only about 10 per cent of the mass was in such environments; the rapid growth to $z = 0$ on these mass scales may well be able to explain the rapid evolution in the global star formation rate. The hypothesis that the growth of structure is largely responsible for the observed decline in star formation with cosmic time (e.g. Lilly et al. 1996) therefore becomes much more attractive.

5 CONCLUSIONS

We have presented a study of seventeen known galaxy clusters, using redshifts and Hα EWs measured from 2dFGRS spectra. We have used this to trace the dependence of relative star formation rates as a function of radius and local density. We conclude as follows.

(i) The distribution of star formation rates is correlated with both distance from the cluster centre and local projected density. The distribution becomes equivalent to that of the global average for radii $\gtrsim 3R_v$, and local projected densities $\lesssim$0.3 times that of the mean cluster virialized region. These results are in good agreement with preliminary results from the Sloan Digital Sky Survey (Gomez et al. 2002).

(ii) The correlation between star formation rate and local projected density holds for galaxies more than two virial radii from the cluster centre. Thus, star formation rates depend primarily on the local density, regardless of their proximity to a rich cluster.

(iii) The conclusion point (ii) means that galaxy transformation is not primarily driven by processes like ram pressure stripping, which only operate in the most extreme environments, but by processes which are effective in lower density, group environments.

(iv) The dependence of star formation rate on density is the same for clusters with $\sigma > 800$ km s^{-1} and for clusters with $\sigma < 800$ km s^{-1}, which implies that the star formation rate is insensitive to the global, large-scale structure in which the galaxy is embedded.

(v) The correlation between star formation and density that is predicted from the morphology–density relation of Dressler (1980) is less steep than observed. This provides conditional support for the view that the correlations with density are due to physical transformation of galaxies in dense regions, and that morphological change occurs on a different time-scale from changes to the current star formation rate. However, it may also be explained by a lower fraction of early type spiral galaxies, relative to late types.

ACKNOWLEDGMENTS

We thank an anonymous referee for useful comments. MLB acknowledges support from a PPARC rolling grant for extragalactic astronomy at Durham. RDP and WJC acknowledge funding from the Australian Research Council. We thank Julio Navarro for providing the numerical simulations, and the Sloan Digital Sky Survey collaboration for sharing their results in advance of publication. We gratefully acknowledge the support of the staff of the Anglo-Australian Observatory for their assistance supporting 2dF throughout the survey, and of the Australian and UK time assignment committees for their continued support for this project.

REFERENCES

Abell G. O., 1958, ApJS, 3, 211
Abell G. O., Corwin H. G., Olowin R. P., 1989, ApJS, 70, 1
Balogh M. L., Morris S. L., Yee H. K. C., Carlberg R. G., Ellingson E., 1997, ApJ, 488, L75
Balogh M. L., Schade D., Morris S. L., Yee H. K. C., Carlberg R. G., Ellingson E., 1998, ApJ, 504, L75
Balogh M. L., Morris S. L., Yee H. K. C., Carlberg R. G., Ellingson E., 1999, ApJ, 527, 54
Balogh M. L., Navarro J. F., Morris S. L., 2000, ApJ, 540, 113
Balogh M. L. et al., 2002, ApJ, 566, 123
Blanton M. R., Dalcanton J., Eisenstein D., Loveday J., Strauss M. A., SubbaRao M., Weinberg D. H., the Sloan collaboration, 2001, AJ, 121, 2358
Bond J. R., Cole S., Efstathiou G., Kaiser N., 1991, ApJ, 379, 440
Bower R. G., 1991, MNRAS, 248, 332
Carlberg R. G., Yee H. K. C., Morris S. L., Lin H., Hall P. B., Patton D. R., Sawicki M., Shepherd C. W., 2001, ApJ, 552, 427
Charlot S., Longhetti M., 2001, MNRAS, 323, 887
Cole S., Lacey C. G., Baugh C. M., Frenk C. S., 2000, MNRAS, 319, 168
Colless M., Dalton G., Maddox S., Sutherland W., Norberg P., Cole S., (the 2dFGRS team), 2001, MNRAS, 328, 1039
Couch W. J., Sharples R. M., 1987, MNRAS, 229, 423

Couch W. J., Balogh M. L., Bower R. G., Smail I., Glazebrook K., Taylor M., 2001, ApJ, 549, 820
Cowie L. L., Songaila A., Barger A. J., 1999, AJ, 118, 603
Cross N. et al., 2001, MNRAS, 324, 825
Dalton G. B., Maddox S. J., Sutherland W. J., Efstathiou G., 1997, MNRAS, 289, 263
De Propris R. et al., 2002, MNRAS, 329, 87
Diaferio A., Kauffmann G., Balogh M. L., White S. D. M., Schade D., Ellingson E., 2001, MNRAS, 323, 999
Domínguez M., Muriel H., Lambas D. G., 2001, AJ, 121, 1266
Dressler A., 1980, ApJ, 236, 351
Dressler A., Thompson I. B., Shectman S. A., 1985, ApJ, 288, 481
Dressler A. et al., 1997, ApJ, 490, 577
Eke V. R., Cole S., Frenk C. S., 1996, MNRAS, 282, 263
Fujita Y., 2001, ApJ, 550, 612
Fukugita M., Shimasaku K., Ichikawa T., 1995, PASP, 107, 945
Geller M. J., Huchra J. P., 1983, ApJS, 52, 61
Girardi M., Giuricin G., Mardirossian F., Mezzetti M., Boschin W., 1998, ApJ, 505, 74
Girardi M., Manzato P., Mezzetti M., Giuricin G., Limboz F., 2002, ApJ, 569, 720
Gomez P. L. et al., 2002, ApJ, submitted
Gunn J. E., Gott J. R. I., 1972, ApJ, 176, 1
Jansen R. A., Fabricant D., Franx M., Caldwell N., 2000, ApJS, 126, 331
Kauffmann G., Colberg J. M., Diaferio A., White S. D. M., 1999, MNRAS, 303, 188
Kennicutt R. C., 1983, ApJ, 272, 54
Kennicutt R. C., 1992, ApJ, 388, 310
Kodama T., Bower R. G., 2001, MNRAS, 321, 18
Kodama T., Smail I., Nakata F., Okamura S., Bower R. G., 2001, ApJ, 562, L9
Lewis I. et al., 2002, MNRAS, 333, 279
Lilly S. J., Le Fevre O., Hammer F., Crampton D., 1996, ApJ, 460, L1
Lumsden S. L., Nichol R. C., Collins C. A., Guzzo L., 1992, MNRAS, 258, 1
Madau P., Ferguson H. C., Dickinson M. E., Giavalisco M., Steidel C., Fruchter A., 1996, MNRAS, 283, 1388
Marzke R. O., Geller M. J., Huchra J. P., Corwin H. G., 1994, AJ, 108, 437
Moore B., Lake G., Quinn T., Stadel J., 1999, MNRAS, 304, 465
Moss C., Whittle M., 2000, MNRAS, 317, 667
O'Hely E., 2000, PhD thesis,Univ. New South Wales
Okamoto T., Nagashima M., 2001, ApJ, 547, 109
Pimbblet K. A., Smail I., Edge A. C., Couch W. J., O'Hely E., Zabludoff A. I., 2001, MNRAS, 327, 588
Pimbblet K. A., Smail I., Kodama T., Couch W. J., Edge A. C., Zabludoff A. I., O'Hely E., 2001, MNRAS, 331, 333
Poggianti B. M., Smail I., Dressler A., Couch W. J., Barger A. J., Butcher H., Ellis R. S., Oemler A., 1999, ApJ, 518, 576
Postman M., Geller M. J., 1984, ApJ, 281, 95
Quilis V., Moore B., Bower R., 2000, Sci, 288, 1617
Sandage A., Tammann G. A., 1981, A Revised Shapley-Ames Catalog of Bright Galaxies. Carnegie Institution, Washington
Solanes J., Manrique A., García-Gómez C., González-Casado G., Giovanelli R., Haynes M. P., 2001, ApJ, 548, 97
Somerville R. S., Primack J. R., 1999, MNRAS, 310, 1087
Sullivan M., Mobasher B., Chan B., Cram L., Ellis R., Treyer M., Hopkins A., 2001, ApJ, 558, 72
Tully R. B., 1987, ApJ, 321, 280
Turner E. L., Gott J. R., 1976, ApJS, 32, 409
Veilleux S., Osterbrock D. E., 1987, ApJS, 63, 295
Whitmore B. C., Gilmore D. M., Jones C., 1993, ApJ, 407, 489

This paper has been typeset from a TEX/LATEX file prepared by the author.